A Journal of the Gesellschaft Deutscher Chemiker
Angewandte Chemie
GDCh
International Edition
www.angewandte.org

Accepted Article

Title: Encapsulating Perovskite Quantum Dots in Iron-Based Metal-Organic Frameworks for Efficient Photocatalytic CO2 Reduction

Authors: Li-Yuan Wu, Yan-Fei Mu, Xiao-Xuan Guo, Wen Zhang, Zhi-Ming Zhang, Min Zhang, and Tong-Bu Lu

To be cited as: *Angew. Chem. Int. Ed.* 10.1002/anie.201904537
Angew. Chem. 10.1002/ange.201904537

Link to VoR: http://dx.doi.org/10.1002/anie.201904537
http://dx.doi.org/10.1002/ange.201904537

WILEY-VCH

10.1002/anie.201904537

WILEY-VCH

Encapsulating Perovskite Quantum Dots in Iron-Based Metal-Organic Frameworks for Efficient Photocatalytic CO_2 Reduction

Li-Yuan Wu, Yan-Fei Mu, Xiao-Xuan Guo, Wen Zhang, Zhi-Ming Zhang, Min Zhang,* and Tong-Bu Lu*

Abstract: Improving the stability of lead halide perovskite quantum dots (QDs) in a reaction system containing water is the key point for their practical applications in artificial photosynthesis. Herein, we encapsulate low-cost $CH_3NH_3PbI_3$ ($MAPbI_3$) perovskite QDs in the pores of earth-abundant Fe-porphyrin based metal organic framework of PCN-221(Fe_x) by a sequential deposition route, to construct a serious of composite photocatalysts of $MAPbI_3$@PCN-221(Fe_x) (x = 0~1). Benefiting from the protection of the framework of PCN-221(Fe_x), the composite photocatalysts exhibit much improved stability in reaction systems containing water. In addition, due to the close contact of QDs to the efficiently catalytic site of Fe in PCN-221(Fe_x), the photogenerated electrons in the confined QDs can swift transfer to the Fe catalytic sites to remarkably enhance the photocatalytic activity of PCN-221(Fe_x) for CO_2 reduction. Using water as an electron source, $MAPbI_3$@PCN-221($Fe_{0.2}$) exhibits a record-high total yield of 1559 μmol g^{-1} for photocatalytic CO_2 reduction to CO (34%) and CH_4 (66%), 38 times higher than that of PCN-221($Fe_{0.2}$) in the absence of perovskite QDs. Our study provides an effective strategy for improving the stability and charge separation efficiency of perovskite QDs, promoting their practical applications in photocatalytic CO_2 reduction.

Direct light-driven CO_2 reduction to high-value added chemical feedstocks or fuels using efficient catalysts is one of fascinating technologies, in response to slowly but inevitably exhausted fossil fuels, as well as the climate-changing induced by CO_2 greenhouse gas emission.[1−6] In above artificial photosynthesis process, a crucial challenge is to design efficient and low-cost catalysts and photosensitizers. In this context, a series of efficient photocatalysts based on earth-abundant elements such as Fe,[7−9] Co[10−13] and Ni[14,15] have been developed.[16] Meanwhile, some semiconductor nanocrystals (NCs) have been pursued as photosensitizers, owing to their large extinction coefficients and flexibly adjustable thermodynamic and optical properties with the regulation of particle sizes.[17−20] In this regard, lead halide perovskite (LHP) NCs are ordinarily endowed with high defect tolerance and long photogenerated carrier lifetime, triggering their widespread applications in photovoltaic and optoelectronic devices.[21−23]

Most recently, LHP quantum dots (QDs) have also been actively pursued as catalysts in photocatalytic fields.[24−33] In photocatalytic CO_2 reduction, LHP QDs have been demonstrated to be capable of converting CO_2 to CO and CH_4.[27] Loading LHP QDs on graphene oxide[26] or g-C_3N_4[24] can facilitate the charge separation, bringing forth improved catalytic performance for CO_2 reduction. However, the insufficient stability of LHP QDs and the lack of effective catalytic sites limit their photocatalytic performance for CO_2 reduction. To overcome these obstacles, we encapsulated LHP QDs of $CH_3NH_3PbI_3$ ($MAPbI_3$) in the pores of Fe-porphyrin based metal organic frameworks (MOFs) of PCN-221(Fe_x) to construct a serious of composite photocatalysts of $MAPbI_3$@PCN-221(Fe_x) for visible-light-driven CO_2 reduction (x = 0~1). Our strategy is based on the following considerations: 1) Owing to the confinement effect of porous MOF, QDs with ultra-small size and homogeneous distribution can be generated in the pores of MOF.[34−37] 2) Apart from good catalytic activity of MOFs for the conversion of CO_2,[34, 38−41] the framework of MOFs can improve the stability of LHP QDs.[37,42] 3) The close contact of LHP QDs to the catalytic active center in MOFs can shorten the charge transfer distance, thus enhancing the photo-induced charge separation efficiency of LHP QDs and catalytic activity of MOFs. As expected, all the $MAPbI_3$@PCN-221(Fe_x) composite photocatalysts exhibit much enhanced photocatalytic stability and activity for CO_2 reduction compared with pure QDs and corresponding PCN-221(Fe_x), getting record-high stability (over 80 h) and yield for the productions of CO and CH_4 (1559 μmol g^{-1}).

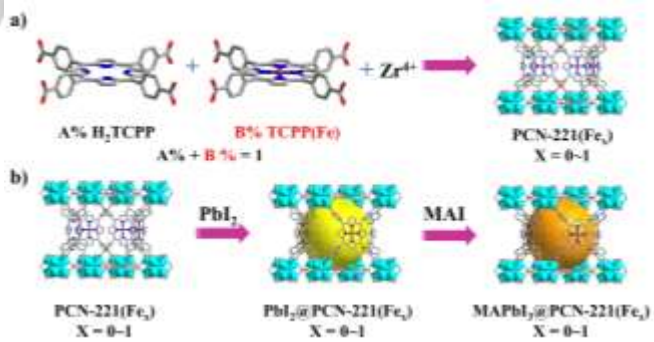

Scheme 1. Schematic illustrations for the synthesis of (a) PCN-221(Fe_x), and (b) $MAPbI_3$ QDs encapsulated in the pores of PCN-221(Fe_x) by a sequential deposition route (MAI = CH_3NH_3I).

As depicted in Scheme 1a, the pristine PCN-221(Fe_x) MOFs with different Fe contents (x = 0, 0.2, 0.4, 0.6, 0.8, 1) were synthesized according to the reported method,[43] and the details are described in the Supporting Information. X-ray powder diffraction (XRD) measurements show that the XRD patterns of PCN-221(Fe_x) are well agree with the simulated pattern of PCN-221 (Figure S1), indicating that the coordination of iron atom to porphyrin ring does not change the crystal

[*] L.Y. Wu, Y.F. Mu, X.X. Guo, Dr. W. Zhang, Prof. Z.M. Zhang, Prof. M. Zhang, Prof. T.B. Lu
Institute for New Energy Materials and Low Carbon Technologies, School of Chemistry and Chemical Engineering,
Tianjin University of Technology
Tianjin 300384, China
E-mail: zm2016@email.tjut.edu.cn; lutongbu@tjut.edu.cn

Supporting information for this article is given via a link at the end of the document.

structure of PCN-221. Considering the fast reaction kinetics of nucleation and growth processes for LHP QDs owing to their ionic crystal feature,[44] we herein performed a sequential deposition route to encapsulate the $MAPbI_3$ QDs into the pores of PCN-221(Fe_x), as illustrated in Scheme 1b. The as-prepared PCN-221(Fe_x) was first immersed in a solution of PbI_2. The resulting PbI_2@PCN-221(Fe_x) was rinsed with *N*,*N*-dimethylformamide/ethanol and ethanol to remove the residual PbI_2 on the surface of PCN-221(Fe_x). PbI_2@PCN-221(Fe_x) was then immersed in a MAI ethanol solution for 10 min to generate the final $MAPbI_3$@PCN-221(Fe_x) composite photocatalysts after rinsing with ethanol. The actual Fe contents in $MAPbI_3$@PCN-221(Fe_x) (x = 0.2, 0.4, 0.6, 0.8, 1) determined by inductively coupled plasma mass spectrometry (ICP-MS) analysis are 0.15, 0.34, 0.55, 0.78 and 0.97, respectively.

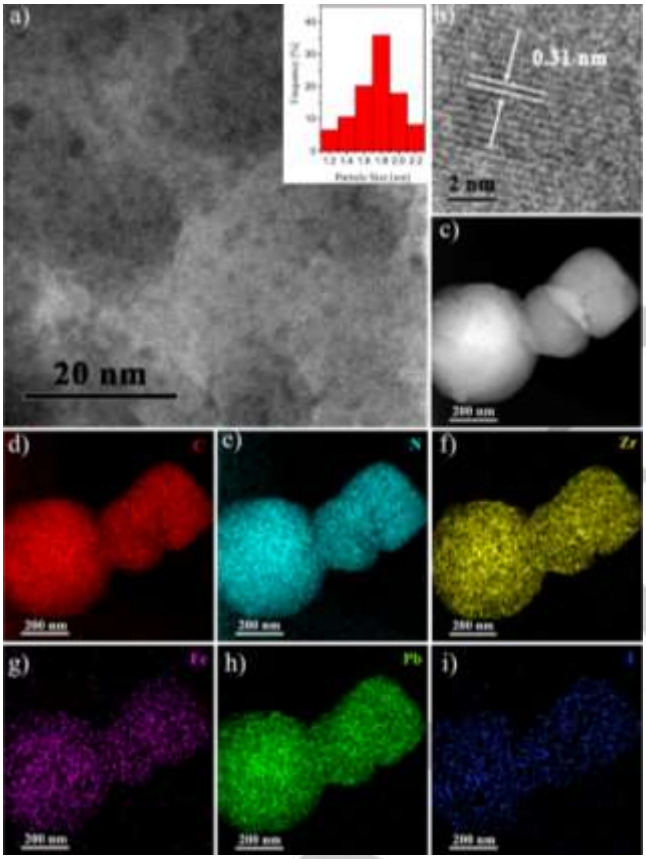

Figure 1. (a) TEM image of $MAPbI_3$@PCN-221($Fe_{0.2}$), the black dots belonging to $MAPbI_3$ QDs, and the inset is particle size distribution of $MAPbI_3$ QDs. (b) HRTEM image with lattice spacing of $MAPbI_3$ QDs in $MAPbI_3$@PCN-221($Fe_{0.2}$). (c) TEM image, and (d-i) elemental mapping for $MAPbI_3$@PCN-221($Fe_{0.2}$).

$MAPbI_3$@PCN-221($Fe_{0.2}$) was chosen as a typical sample to analyse the composition and structure of in-situ generated $MAPbI_3$ QDs within the pores of PCN-221. The results of XRD measurements reveal that the formation of $MAPbI_3$ QDs in the pores of PCN-221($Fe_{0.2}$) does not disturb the framework of PCN-221($Fe_{0.2}$) (Figure S2). The XRD characteristic peaks of $MAPbI_3$ QDs were not observed in $MAPbI_3$@PCN-221($Fe_{0.2}$) composite (Figure S2), which can be ascribed to their small sizes confined in the pores of PCN-221($Fe_{0.2}$). While the IR spectrum of $MAPbI_3$@PCN-221($Fe_{0.2}$) shows the characteristic absorption peaks of $MAPbI_3$ QDs at 1466 and 906 cm^{-1} (Figure S3), which can be assigned to the symmetric bending vibration of NH_3 and rocking vibration of CH_3-NH_3^+, respectively,[45] indicating the existence of $MAPbI_3$ QDs in the pores of PCN-221($Fe_{0.2}$). The TEM image reveals that the average size of $MAPbI_3$ QDs in PCN-221($Fe_{0.2}$) is approximately 1.8 nm (Figure 1a), which matches the pore size of PCN-221($Fe_{0.2}$) (~ 2 nm).[46] HRTEM image of $MAPbI_3$@PCN-221($Fe_{0.2}$) shows the lattice spacing of $MAPbI_3$ QDs being 0.31 nm (Figure 1b), which is consistent with that of $MAPbI_3$ bulky sample.[47] The elemental mapping of $MAPbI_3$@PCN-221($Fe_{0.2}$) (Figures 1d-1i) indicates that $MAPbI_3$ QDs are uniformly dispersed in the pores of PCN-221($Fe_{0.2}$). All the above results demonstrate the $MAPbI_3$@PCN-221($Fe_{0.2}$) composite catalyst was successfully synthesized. The N_2 adsorption isotherms for PCN-221($Fe_{0.2}$) before and after the QDs encapsulation indicate 20% of the pores in the MOF are occupied by $MAPbI_3$ QDs (Figure S4).

The photocatalytic CO_2 reduction reactions were performed in CO_2-saturated ethyl acetate solution containing small amount of water, under 300 W Xe-lamp irradiation with a 400 nm filter. For all the evaluated PCN-221(Fe_x) and $MAPbI_3$@PCN-221(Fe_x) photocatalysts, the main reduction products are CO and CH_4 in the cases of MOFs containing Fe, and CO is the main reduction product for PCN-221 and $MAPbI_3$@PCN-221 without Fe (Figure 2a). No H_2 and liquid products such as HCOOH and CH_3OH were detected for all the evaluated photocatalytic systems. To further confirm the origin of CO and CH_4 products, we first performed control experiments by using N_2 gas to replace CO_2 under the same condition. Almost no CO and CH_4 were produced, as depicted in Figure S5. In addition, $^{13}CO_2$ isotope trace experiment shows that the major mass spectrum signals with m/z values of 29 (^{13}CO) and 17 ($^{13}CH_4$) can be clearly observed (Figure S6), indicating that both CO and CH_4 originate from the photocatalytic CO_2 reduction instead of photo-oxidation of ethyl acetate.

As presented in Figure 2a and Table S1, in the cases of pristine PCN-221(Fe_x) with various contents of Fe as photocatalysts, the CO_2 reduction activity enhances along with the increase of Fe content, owing to the increase of Fe catalytic sites. Moreover, the selectivity of CH_4 formation also increases along with the increase of Fe content in PCN-221(Fe_x) (Figure 2a), which may originate from the increased concentration of CO induced by the enhanced activity, indicating that CO is a key intermediate in the process of CH_4 formation.[8] This speculation has been further demonstrated by the photocatalytic experiment in CO-saturated ethyl acetate/water solution, where CH_4 is the only detected product. However, all the cases of pristine PCN-221(Fe_x) photocatalysts generate very low yields for both CO and CH_4. For the most efficient catalyst system based on pristine PCN-221(Fe), the yields of CO and CH_4 are only 13 and 38 μmol g^{-1}, respectively, after 25 h of irradiation. After that time, the PCN-221(Fe_x) photocatalysts were decomposed and lost the catalytic activity.

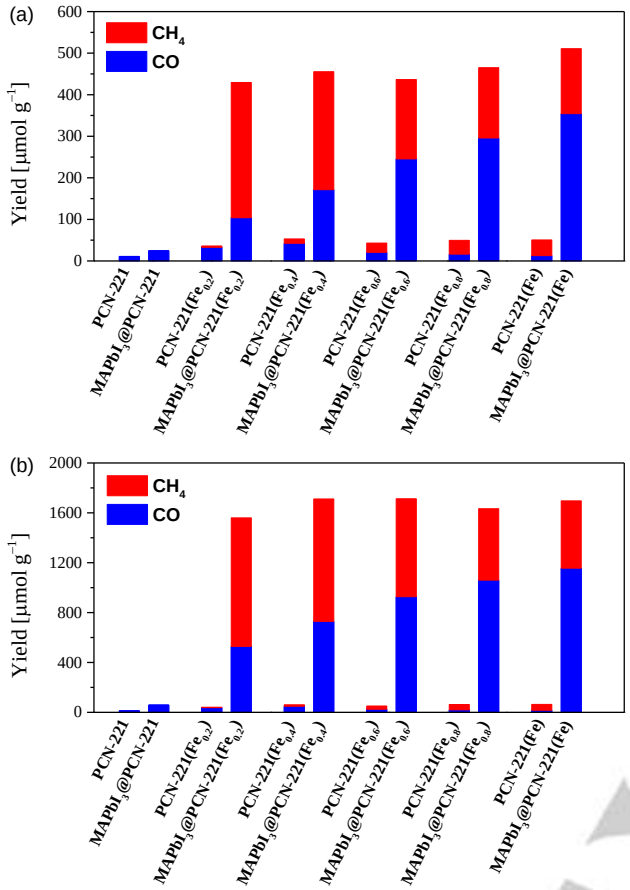

Figure 2. (a) The yields for CO_2 reduction to CH_4 and CO with PCN-221(Fe_x) and $MAPbI_3$@PCN-221(Fe_x) as photocatalysts in the CO_2-saturated ethyl acetate/water solution after (a) 25 h, and (b) 80 h of irradiation under 300 W Xe-lamp, with the light intensity of 100 mW cm^{-2}.

Under the same irradiation time of 25 h, $MAPbI_3$@PCN-221 without Fe also displays little photocatalytic activity for CO_2 reduction (Figure 2a). While the composite photocatalysts containing both $MAPbI_3$ QDs and Fe exhibit significant improvement of photocatalytic activity for CO_2 reduction, generating remarkably enhanced yields for both CO and CH_4, suggesting Fe is the vital catalytic site for photocatalytic CO_2 reduction. Particularly, $MAPbI_3$@PCN-221($Fe_{0.2}$) exhibits the highest photocatalytic activity, achieving 104 μmol g^{-1} of CO and 325 μmol g^{-1} of CH_4. The calculated value for electron consumption rate ($R_{electron}$ = (2Yield CO + 8Yield CH_4)/25 h) is 112 μmol g^{-1} h^{-1}, which is about 31 and 8 times larger than those of corresponding pristine PCN-221($Fe_{0.2}$) and PCN-221(Fe) counterparts, respectively. The values of $R_{electron}$ for $MAPbI_3$@PCN-221(Fe_x) (53 ~ 112 μmol g^{-1} h^{-1}) are also much larger than those of composite photocatalysts of LHP QDs with MOFs coating (15 ~ 30 μmol g^{-1} h^{-1}),[25] which can be ascribed to the close contact between $MAPbI_3$ QDs and Fe catalytic sites. As shown in Figure 2a, the values of $R_{electron}$ and the selectivity of CH_4 generation gradually decrease along with the increase of Fe content in $MAPbI_3$@PCN-221(Fe_x), which may be ascribed to the competitive light absorption between $MAPbI_3$ QDs and PCN-221(Fe_x), resulting in reduced number of transferred electrons from $MAPbI_3$ QDs to Fe catalytic sites along with the increase of Fe content in PCN-221(Fe_x).

Moreover, it is excited to note that the $MAPbI_3$@PCN-221(Fe_x) composite photocatalysts display an obvious improvement of stability compared with relatively stable PCN-221(Fe_x), in which $MAPbI_3$@PCN-221(Fe_x) photocatalysts display linear productions of CO and CH_4 with a time over 80 h, as observed in Figures S5a and S5b, while PCN-221(Fe_x) photocatalysts can only be stable within 30 h (Figures S5c and S5d), after that time they decompose and lose the catalytic activity. Meanwhile, the stability of $MAPbI_3$ QDs in $MAPbI_3$@PCN-221(Fe_x) is also much more stable than those of reported LHP QDs based photocatalysts for CO_2 reduction.[24-27] Thus $MAPbI_3$@PCN-221(Fe_x) composite photocatalysts display significantly enhanced yields for CO_2 reduction, 25~38 times higher than those of corresponding PCN-221(Fe_x) in the absence of perovskite QDs (Figure 2b), in which $MAPbI_3$@PCN-221($Fe_{0.2}$) gets a record-high yield of 1559 μmol g^{-1} for photocatalytic CO_2 reduction to CO (34%) and CH_4 (66%), 38 times higher than that of pristine PCN-221($Fe_{0.2}$) (41 μmol g^{-1}). To the best of our knowledge, this is the highest value among diverse perovskite QDs based catalysts for photocatalytic CO_2 reduction up to now. The results of XRD measurements of $MAPbI_3$@PCN-221($Fe_{0.2}$) and PCN-221($Fe_{0.2}$) after photocatalytic reaction show that the pattern of $MAPbI_3$@PCN-221($Fe_{0.2}$) agrees well with that of simulated PCN-221 (Figure S7), indicating the crystal structure of $MAPbI_3$@PCN-221($Fe_{0.2}$) can retain its integrity after the photocatalytic reaction. While PCN-221($Fe_{0.2}$) becomes amorphous (Figure S7), indicating it totally decomposes after the photocatalytic reaction. The improved stability induced by the insertion of $MAPbI_3$ QDs into the pores of PCN-221($Fe_{0.2}$) may be attributed to the competitive light absorption between $MAPbI_3$ QDs and PCN-221($Fe_{0.2}$), which can decrease the photodegradation of PCN-221($Fe_{0.2}$).[48]

To identify the electron source for the reduction of CO_2 to CO and CH_4, the $H_2{}^{18}O$ isotope trace experiment was carried out in a CO_2-saturated ethyl acetate/$H_2{}^{18}O$ solution containing $MAPbI_3$@PCN-221($Fe_{0.2}$) photocatalyst, and the major mass spectrum signal with a m/z value of 36 ($^{18}O_2$) can be observed (Figure S8). In addition, the amount of oxygen generated in CO_2-saturated ethyl acetate/water solution using $MAPbI_3$@PCN-221($Fe_{0.2}$) as a photocatalyst is close to one fourth of total amount of electron consumption (e_{amount}) for the generation of CH_4 and CO (Figure S9). The above results clearly demonstrate that the electron source for the reduction of CO_2 originates from the oxidation of water rather than the oxidation of ethyl acetate. To further exclude the possibility of the electron source coming from the oxidation of ethyl acetate, a more stable solvent of acetonitrile was used to replace ethyl acetate for the above photocatalytic reaction under the same conditions, and similar amounts of CO, CH_4 and O_2 were also detected (Figure S10). All the above results firmly demonstrate that the electron source for the CO_2 reduction comes from the water oxidation. Our results make a great step forward practical application in artificial photosynthesis using water as an electron source.

To deep understand the origin of the significantly enhanced efficiency for photocatalytic CO_2 reduction induced by capsulation of $MAPbI_3$ QDs into the pores of PCN-221(Fe_x), we

10.1002/anie.201904537

first inspected the light-harvesting capacity of $MAPbI_3$@PCN-221($Fe_{0.2}$) by recording the electronic absorption spectra of $MAPbI_3$@PCN-221($Fe_{0.2}$) and PCN-221($Fe_{0.2}$) powders. As shown in Figure S11, the absorption intensity of $MAPbI_3$@PCN-221($Fe_{0.2}$) is much higher than that of PCN-221($Fe_{0.2}$) owing to the high absorption coefficient of $MAPbI_3$ QDs. In addition, the flat-band potentials (corresponding to the conduction band edge) for PCN-221($Fe_{0.2}$) and $MAPbI_3$@PCN-221($Fe_{0.2}$) obtained from the Mott-Schottky plots are −1.00 V and −1.25 V (vs NHE), respectively (Figures 3a and 3b), indicating the photoexcited electrons in PCN-221($Fe_{0.2}$) have enough driving force to reduce CO_2 to CO (−0.52 V vs NHE) or CH_4 (−0.24 V vs NHE), and the photoexcited electron transfer from $MAPbI_3$ QDs to PCN-221($Fe_{0.2}$) is thermodynamically permissible.

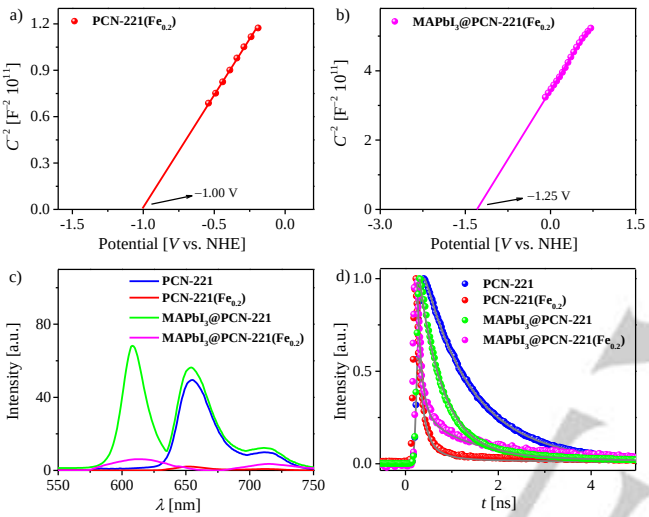

Figure 3. (a) Mott−Schottky plots of $MAPbI_3$@PCN-221 and (b) $MAPbI_3$@PCN-221($Fe_{0.2}$). (c) Steady state photoluminescence spectra of PCN-221, PCN-221($Fe_{0.2}$), $MAPbI_3$@PCN-221 and $MAPbI_3$@PCN-221($Fe_{0.2}$). (d) Time-resolved photoluminescence decays of PCN-221, PCN-221($Fe_{0.2}$), $MAPbI_3$@PCN-221 and $MAPbI_3$@PCN-221($Fe_{0.2}$) with ET519LP as long-wavelength pass filter, after excitation at 375 nm.

Steady state photoluminescence (PL) measurements were further carried out to evaluate the photoexcited electron transfer processes in $MAPbI_3$@PCN-221(Fe_x) composite system. As presented in Figure 3c, PCN-221 shows two peaks around 655 and 712 nm, which originate from the PL of porphyrin groups in PCN-221. The encapsulation of $MAPbI_3$ QDs in PCN-221 leads to a new PL peak at 610 nm, which can be assigned to the luminescence of $MAPbI_3$ QDs. However, the intensities of the above peaks are dramatically decreased in both PCN-221($Fe_{0.2}$) and $MAPbI_3$@PCN-221($Fe_{0.2}$) in the presence of Fe, indicating that the photo-induced electrons transfer rapidly from porphyrin and $MAPbI_3$ QDs to Fe catalytic sites. Furthermore, we also scrutinized the photoexcited charge separation dynamics by recording the time-resolved photoluminescence (TRPL) traces (Figure 3d). The PL traces can be fitted via a multi-exponential function, and the fitting parameters are given in Table S2. As shown in Figure 3d, there is a significantly accelerated PL decay in PCN-221($Fe_{0.2}$) with respect to PCN-221 without Fe ion, with the short time constant τ_1 for electron transfer being only ~ 0.1 ns (Table S2), indicating the occurrence of swift electron transfer from porphyrin groups to Fe catalytic sites after photo-excitation. Moreover, $MAPbI_3$@PCN-221($Fe_{0.2}$) also displays a fast PL decay process compared with PCN-221($Fe_{0.2}$) (Figure 3d), suggesting the time constant of electron transfer from $MAPbI_3$ QDs to Fe catalytic sites is comparable to that from porphyrin groups to Fe catalytic sites in PCN-221($Fe_{0.2}$) (Table S2), which can be ascribed to the close contract between $MAPbI_3$ QDs and Fe catalytic sites.

In summary, $MAPbI_3$@PCN-221(Fe_x) composite photocatalysts have been successfully synthesized based on a sequential deposition route to control the growing rate of $MAPbI_3$ QDs. Encapsulating the $MAPbI_3$ QDs in the pores of PCN-221(Fe_x) does not change their crystal structures, but brings forth an obviously enhanced light-harvesting capacity. Steady state and time-resolved photoluminescence experiments reveal that the photogenerated electrons in the encapsulated $MAPbI_3$ QDs can swift transfer to Fe catalytic sites, achieving efficient charge separation between the perovskite QDs and Fe-porphyrin based MOF. The resultant composite photocatalyst of $MAPbI_3$@PCN-221($Fe_{0.2}$) exhibits extremely high photocatalytic activity for the reduction of CO_2 to CO and CH_4, 38-fold higher than that of corresponding PCN-221($Fe_{0.2}$), using water as a sacrificial reductant. Moreover, the $MAPbI_3$ QDs encapsulation can significantly improve the stability of both LHP QDs and PCN-221(Fe_x). Our study will boost the development of more efficient artificial photosynthesis system based on cheap photosensitizers and earth-abundant catalysts, to reduce CO_2 into chemical feedstocks or fuels using water as an electron source and driven by visible light.

Acknowledgements

This work was financially supported by National Key R&D Program of China (2017YFA0700104), Natural Science Foundation of Tianjin City (17JCJQJC43800), NSFC (21790052, 21722104, and 21702146), and the 111 Project (D17003).

Conflict of interest

The authors declare no conflict of interest.

Keywords: metal organic framework • perovskite quantum dot • Fe-based catalyst • photocatalysis • CO_2 reduction

[1] J. H. Montoya, L. C. Seitz, P. Chakthranont, A. Vojvodic, T. F. Jaramillo, J. K. Nørskov, *Nat. Mater.* **2017**, *16*, 70−81.
[2] J. L. White, M. F. Baruch, J. E. Pander III, Y. Hu, I. C. Fortmeyer, J. E. Park, T. Zhang, K. Liao, J. Gu, Y. Yan, T. W. Shaw, E. Abelev, A. B. Bocarsly, *Chem. Rev.* **2015**, *115*, 12888−12935.
[3] W. Tu, Y. Zhou, Z. Zou, *Adv. Mater.* **2014**, *26*, 4607−4626.
[4] S. Berardi, S. Drouet, L. Francàs, C. Gimbert-Suriñach, M. Guttentag, C. Richmond, T. Stoll, A. Llobet, *Chem. Soc. Rev.* **2014**, *43*, 7501−7519.

[5] S. N. Habisreutinger, L. Schmidt-Mende, J. K. Stolarczyk, *Angew. Chem. Int. Ed.* **2013**, *52*, 7372−7408; *Angew. Chem.* **2013**, *125*, 7516−7557.
[6] M. Cokoja, C. Bruckmeier, B. Rieger, W. A. Herrmann, F. E. Kühn, *Angew. Chem. Int. Ed.* **2011**, *50*, 8510−8537; *Angew. Chem.* **2011**, *123*, 8662−8690.
[7] C. Cometto, R. Kuriki, L. Chen, K. Maeda, T.-C. Lau, O. Ishitani, M. Robert, *J. Am. Chem. Soc.* **2018**, 140, 7437−7440.
[8] H. Rao, L. C. Schmidt, J. Bonin, M. Robert, *Nature* **2017**, *548*, 74−77.
[9] H. Takeda, K. Ohashi, A. Sekine, O. Ishitani, *J. Am. Chem. Soc.* **2016**, *138*, 4354−4357.
[10] Y. Wang, N.-Y. Huang, J.-Q. Shen, P.-Q. Liao, X.-M. Chen, J.-P. Zhang, *J. Am. Chem. Soc.* **2018**, *140*, 38−41.
[11] a) T. Ouyang, H.-H. Huang, J.-W. Wang, D.-C. Zhong, T.-B. Lu, *Angew. Chem. Int. Ed.* **2017**, *56*, 738−743; *Angew. Chem.* **2017**, *129*, 756−761; b) T. Ouyang, H.-J. Wang, H.-H. Huang, J.-W. Wang, S. Guo, W.-J. Liu, D.-C. Zhong, T.-B. Lu, *Angew. Chem. Int. Ed.* **2018**, *57*, 16480−16485; *Angew. Chem.* **2018**, *130*, 16718−16723.
[12] H. Zhang, J. Wei, J. Dong, G. Liu, L. Shi, P. An, G. Zhao, J. Kong, X. Wang, X. Meng, J. Zhang, J. Ye, *Angew. Chem. Int. Ed.* **2016**, *55*,14310−14314; *Angew. Chem.* **2016**, *128*, 14522−14526.
[13] C. Gao, S. Chen, Y. Wang, J. Wang, X. Zheng, J. Zhu, L. Song, W. Zhang, Y. Xiong, *Adv. Mater.* **2018**, *30*, 1704624.
[14] B. Han, X. Ou, Z. Deng, Y. Song, C. Tian, H. Deng, Y.-J. Xu, Z. Lin, *Angew. Chem. Int. Ed.* **2018**, *57*, 16811−16815; *Angew. Chem.* **2018**, 130, 17053−17057.
[15] V. S. Thoi, N. Kornienko, C. G. Margarit, P. Yang, C. J. Chang, *J. Am. Chem. Soc.* **2013**, *135*, 14413−14424.
[16] H. Takeda, C. Cometto, O. Ishitani, M. Robert, *ACS Catal.* **2017**, *7*, 70−88.
[17] J. Wang, T. Xia, L. Wang, X. Zheng, Z. Qi, C. Gao, J. Zhu, Z. Li, H. Xu, Y. Xiong, *Angew. Chem. Int. Ed.* **2018**, *57*, 16447−16451. *Angew. Chem.* **2018**, *130*, 16685−16689.
[18] C. Chen, T. Wu, H. Wu, H. Liu, Q. Qian, Z. Liu, G. Yang, B. Han, *Chem. Sci.* **2018**, *9*, 8890−8894.
[19] M. F. Kuehnel, C. D. Sahm, G. Neri, J. R. Lee, K. L. Orchard, A. J. Cowan, E. Reisner, *Chem. Sci.* **2018**, *9*, 2501−2509.
[20] M. F. Kuehnel, K. L. Orchard, K. E. Dalle, E. Reisner, *J. Am. Chem. Soc.* **2017**, *139*, 7217−7223.
[21] Q. A. Akkerman, G. Rainò, M. V. Kovalenko, L. Manna, *Nat. Mater.* **2018**, *17*, 397−405.
[22] M. V. Kovalenko, L. Protesescu, M. I. Bodnarchuk, *Science* **2017**, *358*, 745−750.
[23] X. Li, F. Cao, D. Yu, J. Chen, Z. Sun, Y. Shen, Y. Zhu, L. Wang, Y. Wei, Y. Wu, H. Zeng, *Small* **2017**, *13*, 1603996.
[24] M. Ou, W. Tu, S. Yin, W. Xing, S. Wu, H. Wang, S. Wan, Q. Zhong, R. Xu, *Angew. Chem. Int. Ed.* **2018**, *57*, 13570−13574; *Angew. Chem.* **2018**, *130*, 13758−13762.
[25] Z.-C. Kong, J.-F. Liao, Y.-J. Dong, Y.-F. Xu, H.-Y. Chen, D.-B. Kuang, C.-Y. Su, *ACS Energy Lett.* **2018**, *3*, 2656−2662.
[26] Y.-F. Xu, M.-Z. Yang, B.-X. Chen, X.-D. Wang, H.-Y. Chen, D.-B. Kuang, C.-Y. Su, *J. Am. Chem. Soc.* **2017**, *139*, 5660−5663.
[27] J. Hou, S. Cao, Y. Wu, Z. Gao, F. Liang, Y. Sun, Z. Lin, L. Sun, *Chem. Eur. J.* **2017**, **23**, 9481−9485.
[28] Y. Wu, P. Wang, X. Zhu, Q. Zhang, Z. Wang, Y. Liu, G. Zou, Y. Dai, M.-H. Whangbo, B. Huang, *Adv. Mater.* **2018**, *30*, 1704342.
[29] S. Park, W. J. Chang, C. W. Lee, S. Park, H.-Y. Ahn, K. T. Nam, *Nat. Energy* **2017**, *2*, 16185.
[30] X. Zhu, Y. Lin, Y. Sun, M. C. Beard, Y. Yan, *J. Am. Chem. Soc.* **2019**, *141*, 733−738.
[31] H. Huang, H. Yuan, K. P. F. Janssen, G. Solís-Fernández, Y. Wang, C. Y. X. Tan, D. Jonckheere, E. Debroye, J. Long, J. Hendrix, J. Hofkens, J. A. Steele, M. B. J. Roeffaers, *ACS Energy Lett.* **2018**, *3*, 755−759.
[32] K. Chen, X. Deng, G. Dodekatos, H. Tüysüz, *J. Am. Chem. Soc.* **2017**, *139*, 12267−12273.
[33] G. Gao, Q. Xi, H. Zhou, Y. Zhao, C. Wu, L. Wang, P. Guo, J. Xu, *Nanoscale* **2017**, *9*, 12032−12038.
[34] L. Jiao, Y. Wang, H.-L. Jiang, Q. Xu, *Adv. Mater.* **2018**, *30*, 1703663.
[35] a) B. Li, J.-G. Ma, P. Cheng, *Angew. Chem. Int. Ed.* **2018**, *57*, 6834−6837; *Angew. Chem.* **2018**, *130*, 6950−6953. b) X.-H. Liu, J.-G. Ma, Z. Niu, G.-M. Yang, P. Cheng, *Angew. Chem. Int. Ed.* **2015**, *54*, 988−991; *Angew. Chem.* **2015**, *127*, 1002−1005.
[36] C. Zhang, B. Wang, W. Li, S. Huang, L. Kong, Z. Li, L. Li, *Nat. Commun.* **2017**, *8*, 1138.
[37] Z. Chen, Z.-G. Gu, W.-Q. Fu, F. Wang, J. Zhang, *ACS Appl. Mater. Interfaces* **2016**, *8*, 28737−28742.
[38] J. W. Maina, C. Pozo-Gonzalo, L. Kong, J. Schütz, M. Hill, L. F. Dumée, *Mater. Horiz.* **2017**, *4*, 345−361.
[39] B. Li, H.-M. Wen, Y. Cui, W. Zhou, G. Qian, B. Chen, *Adv. Mater.* **2016**, *28*, 8819−8860.
[40] A. Dhakshinamoorthy, A. M. Asiri, H. García, *Angew. Chem. Int. Ed.* **2016**, *55*, 5414−5445; *Angew. Chem.* **2016**, *128*, 5504−5535.
[41] T. Zhang, W. Lin, *Chem. Soc. Rev.* **2014**, *43*, 5982−5993.
[42] H. He, Y. Cui, B. Li, B. Wang, C. Jin, J. Yu, L. Yao, Y. Yang, B. Chen, G. Qian, *Adv. Mater.* **2019**, *31*, 1806897.
[43] L. Jiao, G. Wan, R. Zhang, H. Zhou, S.-H. Yu, H.-L. Jiang, *Angew. Chem. Int. Ed.* **2018**, *57*, 8525−8529; *Angew. Chem.* **2018**, *130*, 8661−8665.
[44] I. Lignos, S. Stavrakis, G. Nedelcu, L. Protesescu, A. J. deMello, M. V. Kovalenko, *Nano Lett.* **2016**, *16*, 1869−1877.
[45] T. Glaser, C. Müller, M. Sendner, C. Krekeler, O. E. Semonin, T. D. Hull, O. Yaffe, J. S. Owen, W. Kowalsky, A. Pucci, R. Lovrinčić, *J. Phys. Chem. Lett.* **2015**, *6*, 2913−2918.
[46] D. Feng, H.-L. Jiang, Y.-P. Chen, Z.-Y. Gu, Z. Wei, H.-C. Zhou, *Inorg. Chem.* **2013**, *52*, 12661−12667.
[47] J. Su, D. Lu, L. Zhang, D. Wang, Y. Bai, W. Wang, *Cryst. Res. Technol.* **2017**, 1700171.
[48] J. Bonin, M. Chaussemier, M. Robert, M. Routier, *ChemCatChem* **2014**, *6*, 3200−3207.

10.1002/anie.201904537

WILEY-VCH

Entry for the Table of Contents

COMMUNICATION

Low-cost $CH_3NH_3PbI_3$ ($MAPbI_3$) perovskite quantum dots were successfully encapsulated in the pores of cheap Fe-porphyrin derived MOFs of PCN-221(Fe_x) to construct an efficient photocatalytic system, which displays significantly enhanced catalytic efficiency and stability for visible-light-driven CO_2 reduction using water as an electron source.

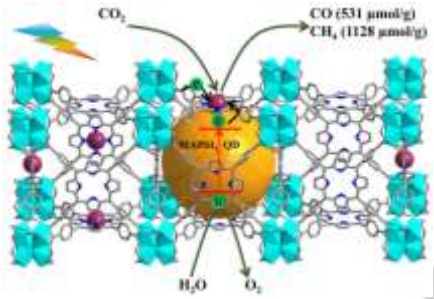

Li-Yuan Wu, Yan-Fei Mu, Xiao-Xuan Guo, Wen Zhang, Zhi-Ming Zhang, Min Zhang, and Tong-Bu Lu**

Page No. – Page No.

Encapsulating Perovskite Quantum Dots in Iron-Based Metal-Organic Frameworks for Efficient Photocatalytic CO_2 Reduction